Research Article
Open Access

3D characterization of the microstructure of LPBF-fabricated Inconel 718 alloy

Abstract

Laser powder bed fusion method is popularly applied in the additive manufacturing of metal parts. The void defect and microstructure are the main factors which determine their mechanical properties. However, the characterization of microstructure and cavities is two dimensional, which is hard to show the spatial profile. In this paper, in order to explore the microstructure and defects in three dimensions, the combined continuously slicing and microstructure observation was used to investigate the microstructure of an Inconel 718 sample. The sample was sliced 468 layers with thickness of 1 µm by xenon ion beam, a 142.8 µm* 107 µm* 46.8 µm microstructure cube was reconstructed. From the 3D model, the melt pool, cavity, pore and grains and their orientations were analyzed. The results provide spatial features of its microstructure. The equi-axed grains are among the coarse column grains, and some are the original grains of insufficiently melt or totally unmelt powder particles. The results tell the difference of the two kinds of voids, i.e., cavity and pore.

Keywords: laser powder bed fusion, Inconel 718, microstructure, 3D characterization, pore, cavity

Volume 7 Issue 1 - 2023

Jinwu Kanga,[1] YuanHang Huangb,[2] Hailiang Yub[2]

[1]School of Materials Science and Engineering, Tsinghua University, Beijing, China
[2]School of Mechanical and Electrical Engineering, Central South University, China

Correspondence: Jinwu Kang, School of Materials Science and Engineering, Key Laboratory for Advanced Materials Processing Technology, Tsinghua University, Beijing, China, Tel +8662784537, Email Kangj@tsinghua.edu.cn

Received: January 26, 2023 | **Published:** February 20, 2023

Introduction

Laser power bed fusion (LPBF), also called selective laser melting (SLM), offers a constraint-free design space to fabricate complex geometries in a single processing step--- track by track and layer by layer.[1,2] The LPBF method can be used for nickel-based alloys, stainless steels, aluminum alloys, copper alloys and titanium alloys for its unique ability to form parts with intricate shapes, high geometrical accuracy and good surface finish.[3–7] The research mainly focuses on the effect of powder and processing parameters on the defects, distortion and residual stress, microstructure and mechanical properties. At least 100 independently controlled processing parameters are involved in the LPBF process,[8] therefore how to optimize the processing parameters to obtain high quality components become the main research focus. The most common and widely studied parameters are laser power P, scanning speed v, hatch spacing d, layer thickness t, and laser spot size.[9–12] These process parameters can be studied individually or using some synthetic process parameter indexes such as energy density, such as linear energy density (P/v), area energy density (P/(vd)), volumetric laser energy density (P/(vdt)).[13–15] The results show there is proper parameters or laser energy density. Zhang et al.,[15] showed that the threshold laser energy density for the Al–Cu–Mg powder is 340 J/mm^3. Too high energy density will also cause void defects as insufficient energy density. An unstable vapor depression zone which finally leads to keyhole forms because of excess laser energy input.[16] Scanning strategy is also a main factor for the density, microstructure and distortion for LPBF. Pant et al.,[17] investigated four different novel scanning strategies representing total fill, re-melting, and two different sectional scanning strategies and found reduced residual stress and variation in crystallographic texture. LPBF is a complex process where the solidification conditions can vary to a great extent. For example, cooling rates in the LPBF process ranges from 10^6K/s ~ 10^8K/s, the melt pool is usually less than 1mm. The solidification microstructural features depend mainly on the melt pool size and solidification conditions (thermal gradient (G) and solidification rate (R)).[18] High thermal gradients and high cooling rates result in the formation of microstructures consisting of high dislocations densities, low angle grain boundaries, sub-granular cellular structures, and crystallographic texture.[19]

Most of research is based on the observation and measurement of specimen surface, thus the spatial features of microstructure such as grains, melt pool and textures are very clear. Although a cube of microstructure was always given in some references, it is actually a fake 3D characterization because it is just the simple pasting of 2D images into the cube surfaces.

In this paper, in order to explore the microstructure and defects in three dimensions, the combined continuous micro slicing and microstructure observation technique is used for the investigation of microstructure and void defect of the as-printed specimen, the results unveils the spatial features of the LPBF fabricated specimen.

Experimental details

A coupon shaped specimen, 15×15×80 mm^3, of Nickel-based Inconel 718 alloy was adopted. The process parameters varied cyclically during printing, where the laser power increased stepwise from 100 W to 210 W in twelve levels, and the scanning speed fluctuated between 500 mm/s and 2000 mm/s in sixteen levels. A total of 63 sets of P-V combinations, with 58 levels of the volume energy density from 50.0 J/mm^3 to 158.0 J/mm^3, as shown in Figure1. Each set of parameters was responsible for eight consecutive layers, thus, a complete cycle consisted of 504 layers. The hatch distance (d) and layer thickness (t) were set as constants at 100 µm and 20 µm, respectively. The fabrication process was conducted on the EP- M100T 3D printer manufactured by Beijing e-Plus 3D Tech. Co. Ltd. (Beijing, China) with highly pure argon gas which was introduced to minimize oxygen contamination. Sixty four identical specimens were designed in eight rows by eight columns on an unpreheated stainless-steel substrate. A raster scan strategy with a rotation of 90 ° in consecutive layers was adopted. The size of the Inconel 718 powder was 10-50 µm. The effect of laser power, scanning speed and the derived laser energy density on microstructure and voids were investigated in reference.[20] However, the microstructure observation is still limited to few horizontal and vertical sections. In this paper, sample No. 34 was cut 35 mm from an as-printed specimen using electrical discharge machining, as shown in Figure 1.

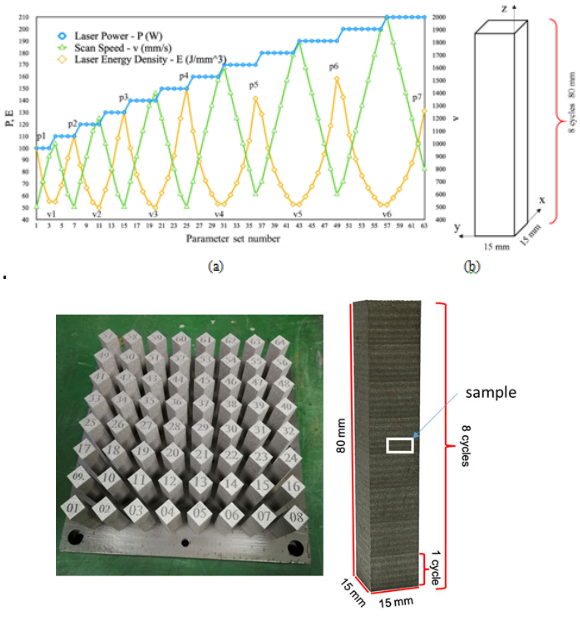

Figure 1 The varying parameters with of laser power and scanning speed (a), the specimen design (b), as-printed specimens on the base plate and a specimen(c) and sample location (d).

The sample was ground, polished and etched using a solution of 1.5 g $CuSO_4$, 40 ml hydrochloric acid and 20 ml alcohol. Macrostructure and microstructure was performed under SEM and optical microscope, and micro hardness was tested, these results were published in reference.[20]

The microstructural analyze was further conducted using a FEI Helios G4 PFIB CXe microscope. The sample was sliced with a thickness of 1µm by xenon ion beam, which is of high micro-milling speed. Then SEM microscope image and EBSD map were taken, the former one for every slice and the later for every other section. The size of each image is 142.8µm* 107µm, the resolution of each EBSD image and SEM image is 714*535 pixels, with each pixel 0.2µm, 2048*1768 pixels, respectively. The section thickness is 1µm. Total 1236 SEM images and 605 EBSD image slices (few EBSD images were missing because of one interruption) are obtained. Roughly 5-7 minutes for each section processing including removing, SEM and EBSD imaging, totally two days was used. A 142.8 µm × 107 µm × 46.8 µm microstructure cube was reconstructed from the top 234 consecutive IPF-Z maps by Avizo software.

The local area around a typical core is cut from the SEM images and then the images were reconstructed by self-developed code which mainly use the open VTK toolkit functions so as to get the geometry of this pore.

Microstructure and void analysis

The IPF-Z maps at different heights are shown in Figure 2 and the 3D constructed model is shown in Figure 3. The Z direction is the printing direction (height). The area of the figure is roughly the size of a melt pool size.

Microstructure

There are equi-axed and columnar grains, however the latter dominates the microstructure with big size and fill the main space, as shown in Figures 2&3. The size of grains also varies a lot. The columnar grains grows mainly along the building direction (Z direction), however, there is a slant angle with the Z direction because the thermal gradient inside the melt pool is radiant from the curved surface toward the center. From the horizontal section, columnar grains can be found, which means these columnar grains is at an angle with the printing direction. The width of the columnar grains are around 2-20µm, the length exceeds the height of the reconstructed cube 46.8 µm.

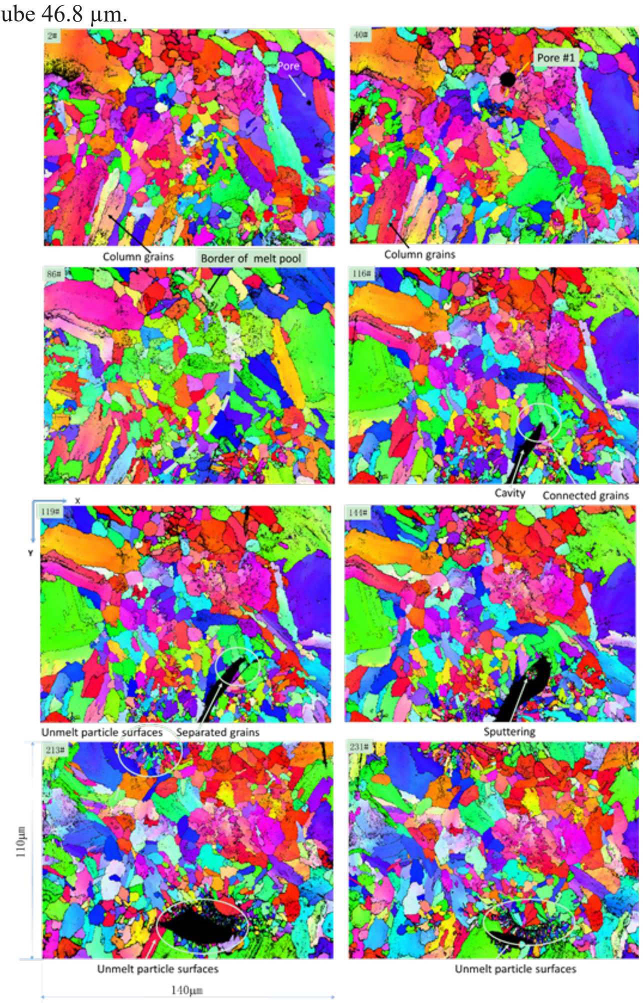

Figure 2 The IPF-Z slice images along z direction, slice sequence numbers are marked at the top left.

There are two kinds of equi-axed grains, one is the original grains of the unmelt powder particles with random origination and of roughly around 2µm, the other is the equi-axed grains among the columnar grains, around 5µm. The unmelt grains are usually located at the bridging area, where the cavities remain after processing. They are also unmelted grains which remain at the core of a powder particle engulfed by the melt pool. It is the result of insufficient melting of a powder particle. The orientations of the grains are random. Inside the columnar grains are cellular dendrites with width in the range of 0.5-1.0µm.[19]

Sputtering, proved by on-axis monitoring[21] can be also seen in the cavities, where tiny particles existed. Inside these particles are fine equi-axed grains around the size of 1µm because of their fast cooling.

From Figure 2 it can be seen that there are grains across the cavity, i.e., with the same orientation although separated. The reason is there are belong to the same grain which can be seen in adjacent slices.

Citation: Kanga J, Huangb YH, Yub H. 3D characterization of the microstructure of LPBF- fabricated Inconel 718 alloy. *Material Sci & Eng.* 2023;7(1):17‒21. DOI: 10.15406/mseij.2023.07.00197

Micro hardness of the grains for all the combinations of parameters varies from 325 to 395 HV,[20] comparable to the values reported in literature with samples fabricated using uniform parameters.[22] Unfortunately the exact value can't be obtained because it is hard to find the parameter set for the current location due to grinding and the thin layer of each parameter set.

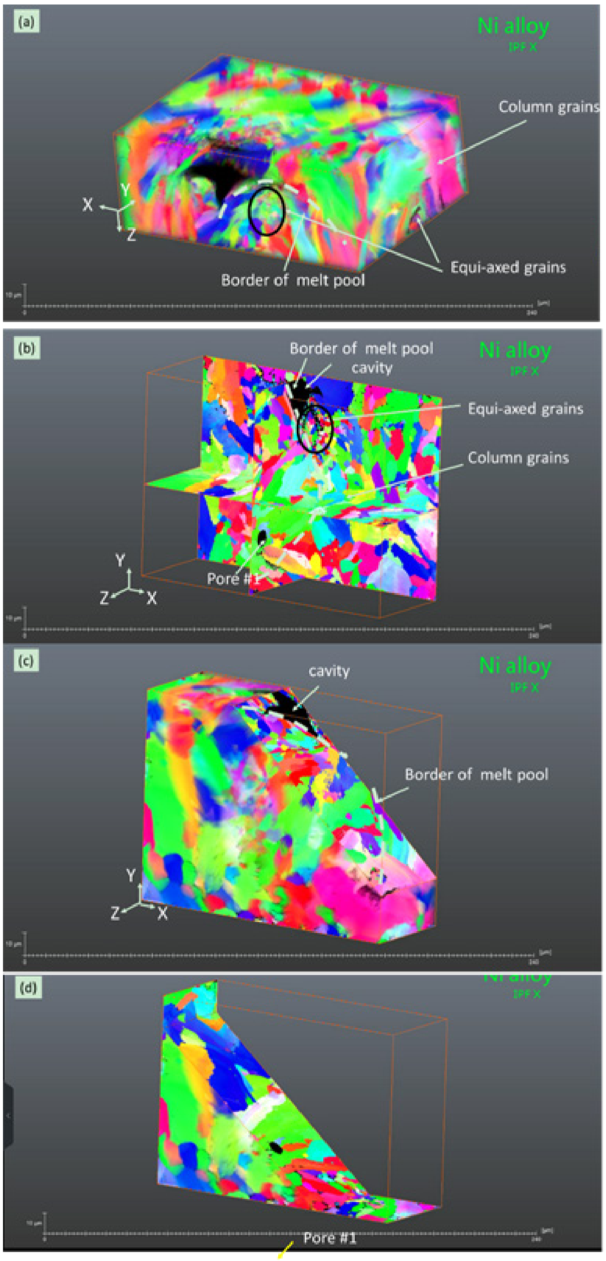

Figure 3 The 3D reconstructed model and sections.

Void

There are two kinds of voids can be seen in Figures 2&3, the cavities among particles, and the pores inside grains. The former one was resulted by the original cavity due to the bridging of powder particles. Although there is certain kind of remelting of particles, the melting was not enough, the original profiles of particles and the package cavity can still be observed.

There are several small pores and a big pore. These pores exhibit circles in the slice with smooth border. And the orientations of the surrounding grains are usually one or two, with the same orientation or very small angle. From the YZ section (Figure 3b) and a slant section (Figure 3d) it is also can be seen the pore #1 section is a circle, which means the pore is a sphere. From some SEM slices a bright point can be seen at the exact center of pore #1, as shown in Figure 4. The bright point is actually the reflection of the bottom of the pore, it only can be seen as the depth is more than the radius of the sphere. In reference[23] tiny bright points are also seen at the center of every round pore, as shown in Figure 5, but it was not discussed. The pores in Fig.6 have two kinds of profiles, with or without a bright reflection point at the center, the ones with a point means the current section plane is higher than their radii, while, the others without a point means the current section plane is lower than their radii. The reconstructed model pore #1 in Figure 2 is given, as shown in Figure 6. It is spherical with smooth internal surface. From the reconstructed 3D model it can be seen the pore is also empty. The bright points don't exist in the IPF map. It also proves the bright point is a reflection of the electrons in SEM image. The sizes varies from 0.08~10µm. The minimum size is limited by the pixel size. The diameter of pore #1 is 9.7µm.

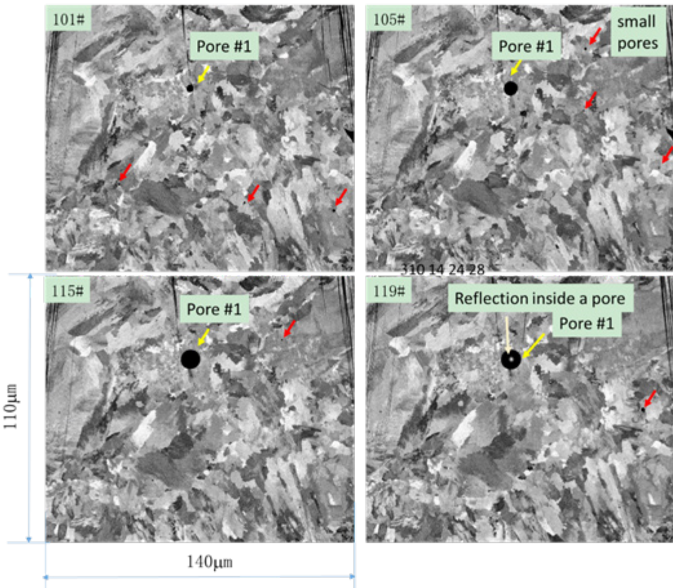

Figure 4 SEM slices images of a pore, reflection can be seen as the section is higher than the radius of the pore.

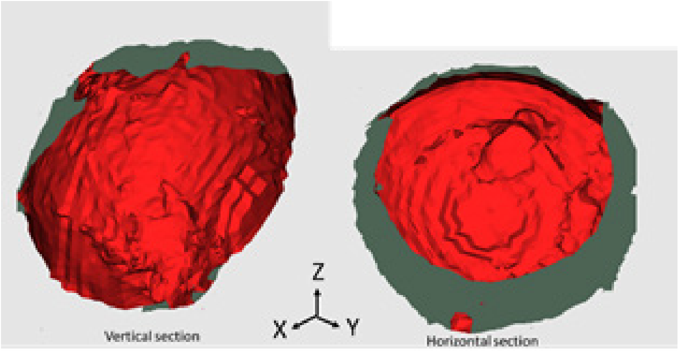

Figure 5 Sections of the 3D reconstructed model of pore #1 with diameter 9.7µm.

Discussion

Columnar grains are the typical microstructure of LPBF fabricated parts, which is the combined result of high energy density, layerwise deposition and high cooling rate. The forming of columnar and

Citation: Kanga J, Huangb YH, Yub H. 3D characterization of the microstructure of LPBF- fabricated Inconel 718 alloy. *Material Sci & Eng.* 2023;7(1):17‒21. DOI: 10.15406/mseij.2023.07.00197

equi-axed grains depends on the G/R, G is the thermal gradient and R is the cooling rare. For LPBF, columnar grains are the typical microstructure. High energy density leads to coarse columnar grains, while, low energy density leads to fine columnar or equi-axed grains. The cavities formed because of insufficient laser energy input. Thus, around the cavities, usually fine equi-axed grains exist, some because of fast cooling, some are the original grains in the unmelt particles. While, coarse columnar grains are found along the center line of melt pool because the melt pool is still of the highest thermal gradient.

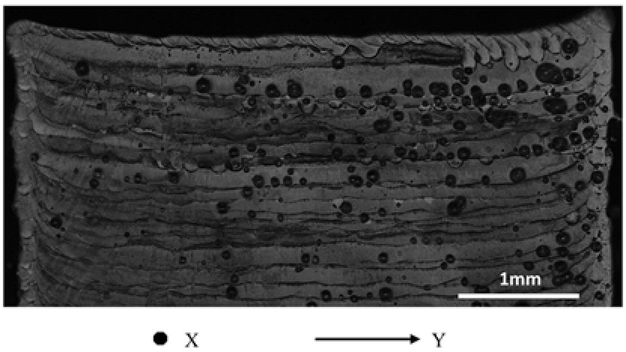

Figure 6 The high laser energy generated many pores on the Inconel 718 alloy sample surface cut along the y-direction.

The cavities among melting tracks vary a lot, from several microns to several hundreds microns, even bigger. It is of the irregular shape, roughly of the gap geometry among round tracks or particles. Therefore, its size and profile lead to its significant effect on mechanical properties than pore. Pore is usually small, less than 10 microns and of round and smooth surface, limited into single grains. And it is proved that they have less effect on the mechanical properties of the LPBF fabricated parts. These pores are formed because the gas dissolved in the melt is released during solidification or entrapped gas.[23] As the melt solidifies, the dissolution content of gas is getting lower and lower, so gas is released from the melt and form a sphere to reduce surface energy. Another explanation is the keyhole caused by the boiling of the melt pool. Su et al.,[24] proved that there is boiling as the pressure of the melt pool which is the sum of all the partial pressure of elements of the melt exceeds the chamber pressure.

However, the size and profile of the left pores change during the keyhole moves forward, the final shape of this kind of pore seems not so smooth,[25] as shown in Figure 7. Usually, as the energy increased to a certain degree, key hole will be significant or the melt pool will be unstable and then result into insufficient overlapping between adjacent melting tracks. For this case, the pore is a perfect smooth, it is more likely the result of released gas from the melt during solidification. Therefore, the optimization of parameters is mainly aiming to reduce the cavities. As the problems of cavities has been controlled, the control of pore will be the future key research problem.

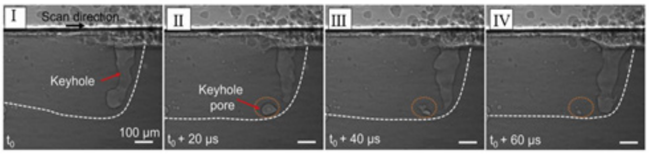

Figure 7 Different pores in AlSi10Mg components by LPBF, keyhole formation collapse at 520W laser power and 0.45m/s scan speed.

The 3D characterization based on ion beam micro-milling is of high resolution of micro region, can be less than 0.1μm, so, the micro pores are possible to be acquired. It is far finer than that by CT based on x-ray or synchrotron x-ray.

Conclusions

The combined sequential slicing and microstructure observation was used to investigate the microstructure of an Inconel 718 sample. A sample is sliced 468 layers with thickness of 1μm by xenon ion beam, a 142.8μm* 107μm * 46.8μm microstructure cube was reconstructed. From the 3D model, the melt pool, cavity, pore and grains and their orientations were analyzed. The results provide spatial features of its microstructure.

1. There are two main kinds of voids, cavity and pores. The former one is of irregular shape, formed among tracks because insufficient layer energy input. Pores are formed inside melt pool and usually inside a simple grain, of sphere shape with smooth surface.
2. The white point in the pore on the slices above the half height of the pore is proved to be the reflection of its smooth bottom. Pore is empty and with smooth internal surface.
3. The microstructure is mainly column grains. Fine equi-axed grains are among the column grains, and some fine equi-axed grains of the insufficiently melt powder particles were kept. The column grains grow from the melt border toward its center at a tilt angle.

Acknowledgments

None.

Funding

None.

Conflicts of interest

There are no conflicts of interest.

References

1. Strößner J, Terock M, Glatzel U. Mechanical and microstructural investigation of nickel-based superalloy in718 manufactured by selective laser melting (SLM). *Advanced Engineering Materials.* 2015;17(8):1099–1105.
2. Yoo YSJ, Book TA, Sangid MD, et al. Identifying strain localization and dislocation processes in fatigued Inconel 718 manufactured from selective laser melting. *Materials Science and Engineering.* 2018;742:444–451.
3. Li R, Liu J, Shi Y, et al. 316L stainless steel with gradient porosity fabricated by selective laser melting. *Journal of Materials Engineering and Performance*. 2010;19:666–671.
4. Jia Q, Gu D. Selective laser melting additive manufacturing of Inconel 718 superalloy parts: densification, microstructure and properties. *Journal of Alloys and Compounds*. 2014;585:713–721.
5. Lu Y, Wu S, Gan Y, et al. Study on the microstructure, mechanical property and residual stress of SLM Inconel-718 alloy manufactured by differing island scanning strategy. *Optics & Laser Technology*. 2015;75:197–206.
6. Mishurova T, Cabeza S, Thiede T, et al. The influence of the support structure on residual stress and distortion in SLM Inconel 718 parts. *Metallurgical and Materials Transactions A*. 2018;49:3038–3046.

Citation: Kanga J, Huangb YH, Yub H. 3D characterization of the microstructure of LPBF- fabricated Inconel 718 alloy. *Material Sci & Eng.* 2023;7(1):17‒21. DOI: 10.15406/mseij.2023.07.00197

7. Ahmad B, van der Veen SO, Fitzpatrick ME, et al. Residual stress evaluation in selective-laser-melting additively manufactured titanium (Ti-6Al-4V) and Inconel 718 using the contour method and numerical simulation. *Additive Manufacturing*. 2018;22:571–582.
8. Yap CY, Chua CK, Dong ZL, et al. Review of selective laser melting:materials and applications. *Applied Physics Revision 2*. 2015;4:041101.
9. DebRoy T, Wei HL, Zuback JS, et al. Additive manufacturing of metallic components – Process, structure and properties*. Progress in Material Science.* 2018;92:112–224.
10. Wei HL, Mukherjee T, Zhang W, et al. Mechanistic models for additive manufacturing of metallic components. *Progress in Material Science.* 2021;116:100703.
11. Fayazfar H, Salarian M, Rogalsky A, et al. A critical review of powder--based additive manufacturing of ferrous alloys: Process parameters, microstructure and mechanical properties. *Material Design.* 2018;144:98–128.
12. Yi JH, Kang JW, Wang TJ, et al. Microstructure and mechanical behavior of bright crescent areas in Inconel 718 sample fabricated by selective laser melting. *Materials & Design.* 2021;197:109259.
13. Deng CY, Kang JW, Feng T, et al. Study on the selective laser melting of cusn10 powder. *Materials.* 2018;11(4):614–620.
14. Zhang XC, Kang JW, Rong YM, et al. Effect of scanning routes on the stress and deformation of overhang structures fabricated by slm. *Materials.* 2019;12(1):47.
15. Zhongshu Ren, Lin Gao, Samuel J, et al. Machine learning–aided real-time detection of keyhole pore generation in laser powder bed fusion. *Material Science.* 2023;379(6627):89–94.
16. Pant P, Salvemini F, Proper S, et al. A study of the influence of novel scan strategies on residual stress and microstructure of L-shaped LPBF IN718 samples. *Materials & Design*. 2022;214:110386.
17. Wang YM, Voisin T, McKeown T, et al. Additively manufactured hierarchical stainless steels with high strength and ductility. *Natural Materials.* 2018;17(1):63–71.
18. Green MOL, Choi CL, Hattrick-Simpers JR, et al. Fulfilling the promise of the materials genome initiative with high-throughput experimental methodologies*. Applied Physics Revision 4*. 2017;4(1):011105.
19. Wang Xiang, Kang Jinwu, Wang Tianjiao. Effect of Layer-Wise Varying Parameters on the Microstructure and Soundness of Selective Laser Melted Inconel 718. Alloy *Materials.* 2019;12(13):2165.
20. Haolin Zhang, Chaitanya Krishna Prasad Vallabh, Xiayun Zhao. Registration and fusion of large-scale melt pool temperature and morphology monitoring data demonstrated for surface topography prediction in LPBF. *Additive Manufacturing.* 2022;58:103075.
21. Deng D, Peng RL, Brodin H, et al. Microstructure and mechanical properties of Inconel 718 produced by selective laser melting: Sample orientation dependence and effects of post heat treatments. *Material Science and Engineering A*. 2018;713:294–306.
22. Su CH, Rodgers K, Chen P, et al. Design processing and assessment of additive manufacturing by laser powder bed fusion: A case study on INCONEL 718 alloy. *Journal of Alloys and Compounds*. 2022;902:163735.
23. Vilaro T, Colin C, Bartout JD. As-fabricated and heat-treated microstructures of the Ti–6Al–4V alloy processed by selective laser melting. *Metallic Materials Transaction.* 2011;10:3190–3199.
24. Hojjatzadeh SMH, Parab ND, Guo Q, et al. Direct observation of pore formation mechanisms during LPBF additive manufacturing process and high energy density laser welding. *Internationa Journal of Machanical Tool Manufacturing.* 2020;153:103555.
25. Kasperovich G, Jan Haubrich, Joachim Gussone, et al. Correlation between porosity and processing parameters in TiAl6V4 produced by selective laser melting. *Materials & Design*. 2016;105:160–170.

Citation: Kanga J, Huangb YH, Yub H. 3D characterization of the microstructure of LPBF- fabricated Inconel 718 alloy. *Material Sci & Eng.* 2023;7(1):17–21. DOI: 10.15406/mseij.2023.07.00197